AIAA JOURNAL
Vol. 41, No. 3, March 2003

Hydrogen and Helium Leak Rates from Micromachined Orifices

I. D. Lee,* O. I. Smith,† and A. R. Karagozian‡
University of California, Los Angeles, Los Angeles, California 90095-1597

Hydrogen is widely in use in rocket propulsion systems, and as such, leakage of hydrogen from high-pressure fuel tanks requires accurate quantification. Safety concerns have led to the practice of conducting leak tests with helium (an inert gas) and to try to infer the hydrogen leak rates from helium data, often employing assumptions of essentially isentropic flow processes and choked leak orifices. The experimental study sought to quantify precisely the relationships between hydrogen and helium leak rates for various types of leaks. Simulated leak sources were fabricated by micromachining leaks or holes of prescribed shapes and cross-sectional areas in silicon wafers, utilizing the processes of photolithography and deep reactive ion etching. Dual thermal conductivity detectors were used to evaluate helium and hydrogen leak rates and to quantify differences in discharge coefficients among the various microorifices. Based on this quantification, the standard helium signature test procedure was found to underpredict hydrogen leak rates, in some cases significantly, if the corresponding helium tests are conducted at much lower pressures than those at which hydrogen leak rates are sought.

Nomenclature

A_{orifice}	=	effective cross-sectional area of leak source
DC	=	discharge coefficient representing dissipation [Eq. (3)]
d_{hyd}	=	orifice hydraulic diameter
Kn	=	Knudsen number, λ/L
L	=	characteristic length
m	=	molecular mass of gas species
$\dot{m}$	=	mass flow rate
p	=	static pressure
p_t	=	stagnation pressure
R	=	gas constant, $\Re/m$
$\Re$	=	universal gas constant
Re_d	=	Reynolds number $(\rho U d)/\mu$
T_t	=	stagnation temperature
U	=	bulk velocity
γ	=	ratio of specific heats, c_p/c_v
λ	=	mean free path
μ	=	absolute viscosity
ρ	=	gas density

Introduction

ROCKET engines often utilize hydrogen as the primary fuel source because of the benefits one derives from hydrogen's combustion properties. As compared with hydrocarbon fuels, hydrogen–oxygen reactions produce high flame speeds and high engine specific impulse, whereas hydrogen is readily storable in the condensed phase. Unfortunately, gaseous hydrogen has a very low flammability limit and low ignition energy, so that it becomes a very dangerous and volatile substance to work with during the rocket engine development stage. Hydrogen leakage into an oxidizing environment can easily ignite a catastrophic explosion. Thus, development of accurate hydrogen leak detection techniques is critical for safety as well as a robust design process.

Typical leak detection methods are generally categorized as point source detection methods and systematic detection methods. Point source detection methods include ultrasonic leak detection, bubble checks, discrete thermal conductivity gas detection, joint bagging, and mass spectroscopy conducted at system joints. They employ conventional as well as novel optical or solid-state hydrogen sensor systems.[1–3] These methods are useful tools for locating discrete leak sources. However, point source detection methods alone cannot guarantee leak proof systems because 1) a user must guess a possible leak point location and 2) very small leaks, below the detection limit of the measuring device, can build up and result in large fuel concentrations within the system over time.

Systematic detection methods, also called concentration assessment methods, are used to make time-resolved fuel concentration measurements within a closed volume. The system's safety status is determined based on the fuel concentration before hot-fire testing. Systematic detection methods include implementation of conventional oxygen and hydrogen sensors as well as more recent microelectronic hydrogen sensors.[4] The helium signature test (HST) is another widely used and well-known systematic detection technique, and it was developed to verify the safety of the space shuttle main propulsion system during the 1980s (Ref. 5). The HST was also used in connection with more recent NASA Linear Aerospike SR-71 Experiment tests of the Lockheed Martin X-33 vehicle.[6,7]

The HST procedure described here is based on the discussion by Hass et al.[6] The HST consists of a two-step experiment involving a pressurized helium tank and propellant feed system contained within a chamber into which nitrogen can be injected. In the first step, with the valve to the pressurized helium tank closed, gaseous helium with a known flow rate is purged at specific locations along the feed system that have the highest possibility of fuel leakage during the operation. Injection of known rates of nitrogen, along with the known flow rates of helium in the system, then allow correlations between helium concentrations and mass spectrometer readings to produce calibration curves. The second step of the HST involves pressurizing the gaseous helium in the tank and then allowing it to flow through the propellant feed system. This process is performed at various tank pressures, but the pressures used are generally much lower than the typical operating pressures for rocket engines; in some cases, tests are conducted at pressures that are one to two orders of magnitude lower than for typical rocket engines.[6] The mass spectrometer's helium calibration curves then allow quantification of the helium mass flow rate $\dot{m}_{\text{He}}$ due to leakage in the system.

The cross-sectional area of the leak source(s), A_{orifice}, may then be calculated from knowledge of the measured helium leak rate $\dot{m}_{\text{He}}$ and from an isentropic flow relation that assumes a choked (sonic) flow at the leak source and a short (thin) leak path:

$$A_{\text{orifice}} = \frac{\dot{m} T_t^{\frac{1}{2}}}{f(\gamma, R) p_t} \tag{1}$$

Received 7 September 2001; revision received 2 July 2002; accepted for publication 22 August 2002.

*Graduate Student Researcher, Department of Mechanical and Aerospace Engineering; currently R&D Engineer, Thermal Engineering, Loral Space and Communications, Ltd., Palo Alto, CA 94303.

†Professor, Department of Mechanical and Aerospace Engineering.

‡Professor, Department of Mechanical and Aerospace Engineering; ark@seas.ucla.edu. Associate Fellow AIAA.

where $\dot{m}$ is the mass flow rate of gas exiting from a pressurized tank through the leak or orifice, T_t and p_t are the stagnation temperature and pressure, respectively, within the tank upstream of the leak orifice, and $\gamma = c_p/c_v$ is the ratio of specific heats for the gas. The function $f(\gamma, R)$ takes the form

$$f(\gamma, R) = (\gamma/R)^{\frac{1}{2}}[2/(\gamma+1)]^{(\gamma+1)/2(\gamma-1)} \tag{2}$$

For helium, γ takes the value 1.66, and the gas constant $R_{He} = 386.04$ ft · lbf/(lbm · °R) [2.077 kJ/(kg K)].

Once $A_{orifice}$ has been estimated for the helium leak source, the leak rate for hydrogen in an equivalent system, but at a higher tank pressure p_t, is estimated using $\gamma_{H2} = 1.4$ and the gas constant $R_{H2} = 766.53$ ft · lbf/(lbm · R) [4.124 kJ/(kg K)]. Equation (1) is used once more to calculate the corresponding hydrogen mass flow rate $\dot{m}_{H2}$ associated with the same leak source area $A_{orifice}$, but at a higher stagnation pressure (one of practical interest). The hydrogen mass flow rate $\dot{m}_{H2}$ is then used, with knowledge of the nitrogen mass flow rate $\dot{m}_{N2}$ in the system, to calculate the hydrogen concentration by volume, which can then be compared to an acceptable concentration or leak limit. In accord with NASA's flight safety rules, the accepted hydrogen leak limit before hot-fire testing is conducted is 1% by volume.[6]

There are a number of problems with the HST that have been identified by NASA.[6] The flow physics associated with the leak process are not clear because the sizes of leak sources may be at the scale of micrometers to tens of micrometers. As a result, it is not known whether or not the flow through the leak is even in the continuum regime. Moreover, because Eq. (1) assumes isentropic flow between the tank and the orifice exit, a discharge coefficient (DC) is required to represent dissipative effects. It is not known if different types of leak orifice shapes have the same effective DC values. A DC can be defined, for example, by a modification of Eq. (1):

$$\dot{m} = \mathrm{DC}\left(A_{orifice}\, p_t \Big/ \sqrt{T_t}\right) f(\gamma, R) \tag{3}$$

Thus, use of Eq. (1) as the means to correlate helium and hydrogen leak rates in the HST requires verification of the following issues. First, it is desired to know if the flow at the leak source is really choked. Jackson[8] has verified that flow through a small but relatively thick circular orifice [with a diameter of about 0.18 in (4.6 mm)] does actually become choked if the ratio of the downstream pressure to upstream stagnation pressure lies below the critical pressure ratio,

$$(p/p_t)_{critical} = [2/(\gamma+1)]^{\gamma/(\gamma-1)} \tag{4}$$

It is not clear, however, that choked flow arises when Eq. (4) is satisfied yet when the orifice diameter is of the order of tens of micrometers. Furthermore, the nature and typical sizes of the discharge coefficient in Eq. (3) are needed as a means of testing the HST's isentropic assumption. Finally, and most important, it is desired to validate whether or not hydrogen leak rates from high-pressure storage tanks may indeed be inferred from helium leak rates from tanks at lower pressures.

To our knowledge, little or no previous work has been done on such high-pressure gas flows in micrometer-scale orifices. As noted, Jackson[8] observes choked behavior in relatively small circular orifices when the pressure ratio across the orifice is less than or equal to the critical value. Choked behavior is considered to occur here when the discharge coefficient asymptotes to a constant value as the pressure downstream of the orifice is reduced. Jackson does find, however, that this asymptotic behavior only occurs for orifices machined into relatively thick plates (with plate thickness greater than the orifice diameter). When the orifice is situated in a very thin plate or "knife-edged" device, even when the pressure ratio is smaller than the critical condition, the discharge coefficient continues to change. Jackson thus concludes that the condition in Eq. (4) may not provide an adequate verification of choked flow for orifices in thin plates. Cunningham[9] similarly suggests that choked flow does not occur across a standard, thin, square-edged orifice.

Molecular effects often cannot be ignored in flows within microscale devices and orifices because the sizes of the gas or liquid molecules and the length scales in the device can become comparable. Hence, commonly used boundary conditions for flows in the continuum regime, such as the "no-slip" condition for viscous flow adjacent to a solid surface, break down when molecular effects are important. In general, flows in which molecular effects become important can be determined theoretically by the size of the Knudsen number $Kn = \lambda/L$, where λ is the mean free path of a molecule and L is a characteristic length scale in the flowfield. Typically, for $Kn < 0.01$, the continuum approximation, and hence the no-slip boundary condition, are valid, whereas for $0.01 < Kn < 0.1$, slip effects need to be represented, and for $Kn > 1$, the flow is said to be in the free molecule regime.[10]

Ho and Tai[11] and Shih et al.[12] have examined this slip condition for compressible flows in microchannels. Their findings suggest that the actual measured mass flow rate in a channel of height 1.2 μm and width 4000 μm is higher than would be predicted from the pressure gradient using the no-slip boundary condition in the solution of the Navier–Stokes equations. When molecular slip is represented in the channel analysis, however, good correspondence with experimental data is obtained. Because these results pertain to flows generated by relatively low-pressure drops, it is not clear that these microfluidics results are directly applicable to the high-pressure fuel tank-generated orifice flows in the present problem.

The present study thus sought to answer questions pertaining to flow regime, choked flow, and general validity of the NASA HST by performing direct mass flow rate comparisons. Micrometer-scale leak orifices with known geometries and cross-sectional areas were manufactured and used to compare flow rates of gaseous helium and hydrogen originating in high-pressure storage tanks. Thus, leak rates could be compared between hydrogen and helium and compared among orifices of various shapes and cross-sectional areas. In addition to the quantification of DCs and verification of the HST method, it was possible to begin to quantify and understand the physics of flows through microscale orifices and channels.

Experimental Configuration

Figure 1 displays a diagram of the system configuration for the present experiments. High-pressure gases (helium and hydrogen) were stored in separate tanks, at point 2 in the diagram, at pressures that were regulated from 1.0 to 13.65 atm. Either test gas could be introduced into a channel in which a 250-μm-thick silicon wafer, with a hole or orifice of prescribed shape and cross-sectional area, was mounted (at point 1 in Fig. 1). Hydrogen or helium gas leaked through the orifice at rates dependent on the pressure difference between the tank and the line flow downstream of the orifice, as well as the orifice geometry. The leaked gas then mixed with nitrogen gas metered into the system at a known flow rate and pressure. The mixture traveled into a dual thermal conductivity detector (TCD) (SRI model 100), which measured, through comparison with a stream of pure nitrogen, the concentration and, hence, the flow rate of the leaked gas (helium or hydrogen) in the mixture.

The TCD had a detection limit of around 100 ppm. Its calibration was conducted using eight calibration gases (four different concentrations for each of two gases, He and H_2) and a wide range of sample concentrations, ranging from 700 to 100,000 ppm. Two flow controllers were installed in the system to maintain flow to the TCD at a constant rate, on the order of 10 ml/min. A pressure relief valve was installed in the system (connected at point 3 in Fig. 1) to maintain a constant nitrogen carrier gas pressure at 3.04 atm, while also contributing to control of the nitrogen carrier gas flow (which was measured by a Tylan FC260 electronic mass flow meter/controller). Typical mass flow rates of the carrier gas were in the range of 4–7 standard l/min to minimize the time until the system reached steady state.

A specially designed flange was used to hold the micromachined silicon orifices at the measuring position (point 1 in Fig. 1). The flange was carefully designed and tested to eliminate leaks to the atmosphere and around the silicon test wafer. An 8-bit data acquisition and control board was used to record the helium and hydrogen concentration data. A single measurement took about 1.5 min, depending on the frequency and the number of data points required.

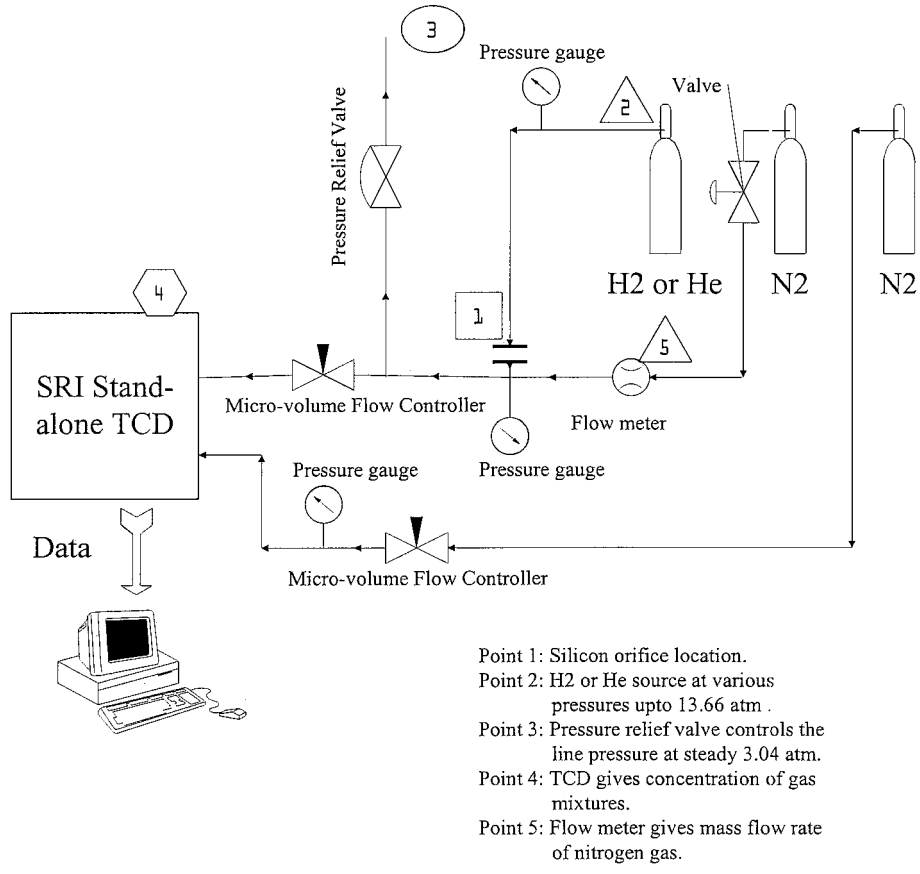

Fig. 1 Schematic diagram of experimental system for measurement of hydrogen and helium concentrations in nitrogen.

The flow rates in the mixture sample line and the carrier gas line were measured and matched so that both lines had a constant 10-ml/min flow rate at all times. A solid silicon wafer of 250-μm thickness, without a hole, was used to check for diffusion of gas through the wafer and for leakage about the flange. Repeated test results showed no trace of any leakage of either the helium or hydrogen sample gas. Pressures were measured at two locations: 1) upstream of the leak or microorifice with a pressure gauge connected to the sample gas regulator, near point 2 in Fig. 1, and 2) downstream of the orifice, at a three-way-low-dead-volume connector, where the sample gas mixed with the nitrogen carrier gas flow. Although this pressure measurement location was not immediately downstream of the microorifice, the downstream pressure (maintained at 3.04 atm) was only used in the computation of sample gas flow rates when it had been determined that the flow through the orifice was not likely to be choked (see Results section).

Microfabrication of Prescribed Leaks

A standard lithography method, followed by the deep reactive ion etching (DRIE) technique, was used to manufacture microorifices of prescribed shapes and cross-sectional areas in the silicon wafers. The goal was quite simple: to manufacture orifices of prescribed shapes with the smallest possible bore dimension on the thickest possible silicon wafer to sustain structural integrity when exposed to normal and shear stresses. Thus, very high-aspect-ratio etching of the holes was inevitably required, where the aspect ratio is that of the etched hole depth to the width or other characteristic length scale. High-aspect-ratio etching imposed some technical difficulties, and as a consequence, slight modifications to the standard procedures were required to achieve the state-of-art limits for DRIE.[13] Details on the complete photolithography and DRIE processes used here may be found in Ref. 14.

Before the initiation of the photolithography process, a photomask with a variety of different microorifice templates (of varying sizes and shapes) was designed and drawn, using AutoCAD, in preparation for professional manufacturing. A photomask is the equivalent of a photographic negative, consisting of a light-sensitive polymer that rests on a layer of chromium and a glass substrate. The mask was designed in the present experiments to be symmetric, so that double-sided etching could be attempted as well, that is, where etching from opposite sides of the wafer creates a single hole. A representation of the photomask used in the present experiments is shown in Fig. 2. The entire photomask was 10.16 cm in diameter. Each circular wafer template within the mask was 1.27 cm in diameter, and each of these contained a microorifice template. Eight rectangular boxes were placed at the edges of the mask to measure the etched bore depth.

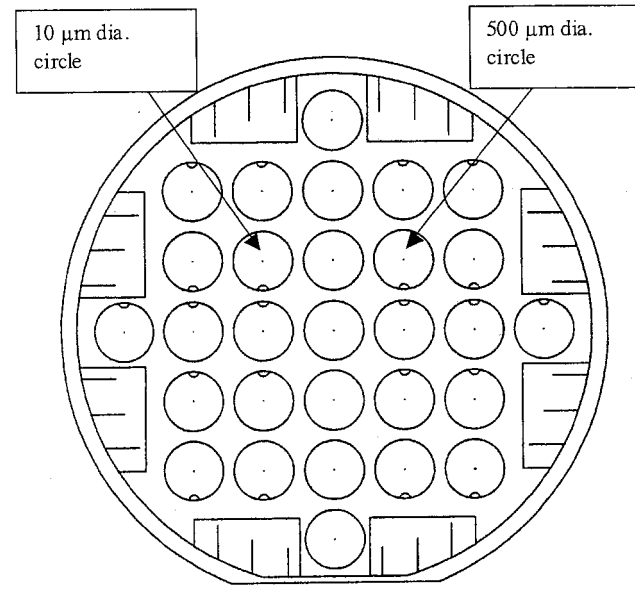

Fig. 2 Photomask used to perform photolithography and DRIE; masks used to create 10-μm-diam circle and, when turned over, 500-μm-diam circle on back of wafer are labeled.

Table 1 Geometrical length scales of the micromachined orifices explored

Orifice	A, μm	B, μm	C, μm	D, μm	E, μm	F, μm	G, μm
1 (Circle)	10	15	20	30	40	50	70
2 (Square)			18	27	35	44	62
3 (Slit)				(15, 35)	(15, 72)	(15, 119)	(15, 245)
4 (Slit)						(35, 29)	(35, 85)

A total of 18 different kinds of orifices were designed on the photomask. The design dimensions (in micrometers) and characteristics are shown in Table 1. The numbered rows represent various orifice shapes, and the lettered columns represent orifices with approximately equivalent cross-sectional areas. For example, the orifice labeled 1A represents an orifice with a 10-μm diameter, circular shaped bore, whereas 2C represents a square orifice with 18-μm sides. Because orifices of different shapes but the same cross-sectional area could be studied, we could investigate the effect of leak shape as well as size on discharge coefficient [defined in Eq. (3)]. Note that slit orifices of dimensions (A, B) given in Table 1 were actually elongated rectangles of length B and width A with semicircular caps of diameter A at each end.

The standard photolithography process, including DRIE of the microorifice, is shown schematically in Fig. 3. Before the spin coating noted in the schematic, a hexaethyl disilazane vapor prime was applied to the silicon wafer. Spin coating of a photoresist layer (AZ4903) onto the 250-μm-thick silicon wafer was then required to achieve accurate etching of holes in the silicon surface by ions during the (later) DRIE stage. The photoresist layer, a photosensitive coating of organic polymer, prevents uncontrolled etching by ions at the top of the silicon layer. Spin coating in the present experiments was performed at 1500 rpm for 40 s. This resulted in the deposition of a photoresist layer of about 25 μm in thickness, which was sufficient for about 1100 DRIE cycles. After a delay of about 3 min to allow the photoresist layer to equilibrate, the element, consisting of the photoresist and the silicon wafer, was soft baked at 120°C for 5 min. Soft baking in general ensures that the photoresist does not stick to the photomask, which is placed on the top of the element during the exposure phase.

The exposure step consisted of exposing the photomask, photoresist, and silicon wafer (Fig. 3) to UV radiation at 400 mJ/cm^2. This was performed in the present experiments using a Karl Suss MA-6 mask aligner, which aligned the mask and photoresist during exposure. The UV light shone through the chromium photomask, focusing the orifice image and circular wafer template through a lens onto the photoresist. The parts of the photoresist struck by the UV light were, thus, selectively removed in the shapes of the designed orifice patterns. After exposure to the UV light, the element was then exposed to a developing fluid, AZ400K, which was mixed with water in the proportion 1:2.5 (AZ400K:water). This developing step was performed for 60 s, with the aim of further selectively removing the photoresist. A supporting silicon wafer is typically attached to the back of the sample silicon wafer, shown in Fig. 3, to prevent gas leakage through the holes during the etching process; this phenomenon could suspend further etching. After these steps, the wafer was ready for the DRIE process.

DRIE is usually performed in a high-density plasma etcher such as a reactive ion etching (RIE) machine. The plasma working fluid typically consists of fluorine ions and atoms produced from sulfur hexafluoride, which was used in the present studies. RIE has many advantages over conventional etching techniques; these include high etch rates, good selectivity, and anisotropy. The anisotropy characteristic refers to the formation of a vertical sidewall profile during etching, and it is one of the most useful characteristics of DRIE. Aspect ratio nonuniformities can occur in these processes, however, because, as ions etch away the silicon layer, the etching rate decreases with the depth of the etch. In the present experiments this caused a tapering of the orifice during the etch, so that the orifice at the top of the wafer was sometimes greater in size than that at the bottom. This problem was eliminated by 1) increasing the etching time and, hence, using relatively thick photoresist layers, of the order 25 μm, 2) optimizing the concentration of the developing fluid (producing that indicated earlier), and finally 3) performing double-sided etching of orifices.

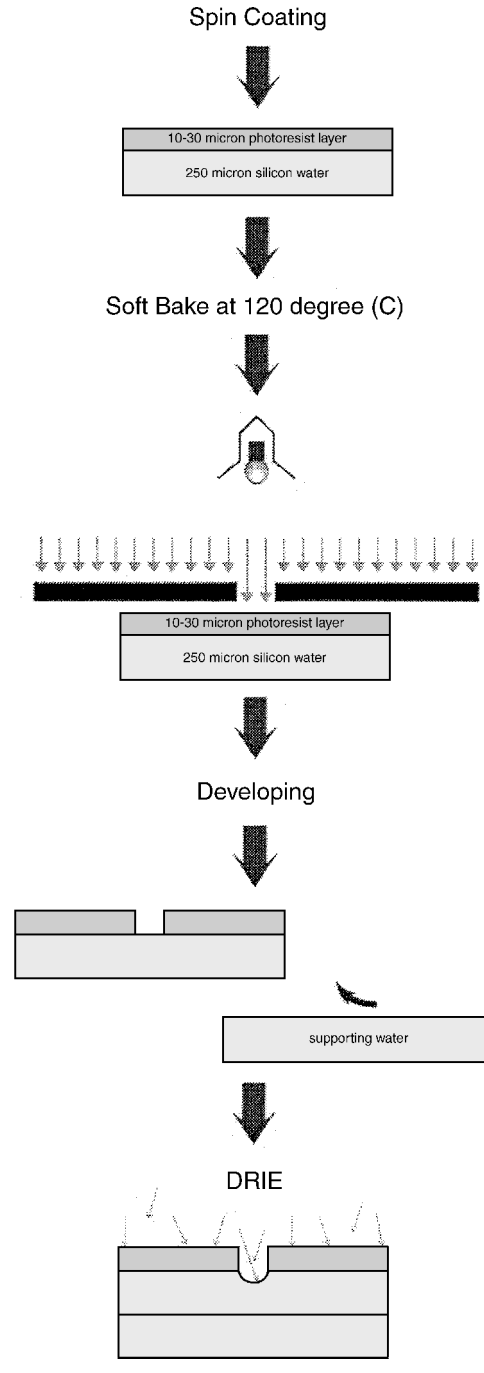

Fig. 3 Standard photolithography process for micromachining leak orifices, including spin coating of the photoresist layer on the silicon wafer, soft bake process, application of UV light to the photomask (in black) and photoresist, the development stage, and the DRIE process.

Double-sided etching, whereby the photolithography and DRIE process is applied to both sides of the silicon wafer, is typically used to produce deep holes or trenches and, hence, large aspect ratio holes. In the present experiments, single-sided etching permitted machining of circular orifices with diameters as small as 20 μm in a 250-μm-thick silicon wafer. The same steps as outlined in Fig. 3, involving photolithography and DRIE, were followed in the double-sided etching procedure, except that during photolithography of the first side the supporting wafer was not needed because the wafer was not etched all of the way through. Alignment errors introduced by etching the silicon from both sides were of the order 1–2 μm. Such errors were relatively small for larger holes, but for holes with hydraulic diameters below 20 μm, these alignment errors could be significant. As a consequence, for the smallest orifices (1A and 1B

in Table 1), the double-sided etching technique was used, but with a different orifice size on either side of the wafer. On one side, for example, a 10-μm-diam circular orifice was etched for a depth of 70 mm, whereas on the other side of the wafer, a 500-μm-diam circular orifice was etched for a depth of 180 μm. The same process was used to produce a 15-μm-diam circular orifice. The resulting wafer, shown schematically in the left side of Fig. 4, allowed examination of much smaller holes than could be accomplished in the 250-μm-thick silicon wafers, shown schematically on the right-hand side of Fig. 4.

Sample photographs of the orifices micromachined via the double-sided etching technique are shown in Figs. 5 and 6. These photographs were taken by an optical microscope with a 400× magnification. As a result of the double-sided etching technique, relatively uniform bore shapes were observed in both top and bottom views of the circular and elliptical (or slit) orifices.

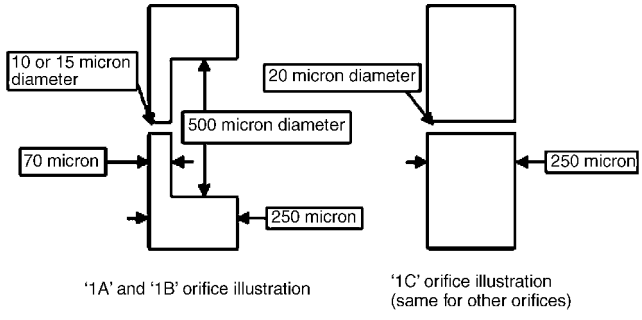

Fig. 4 Side views of the orifices machined by etching from both sides of the silicon wafer: left orifice of 10- or 15-μm diameter with a 70-μm thickness and right orifice of 20-μm or greater diameter with a 250-μm thickness configuration.

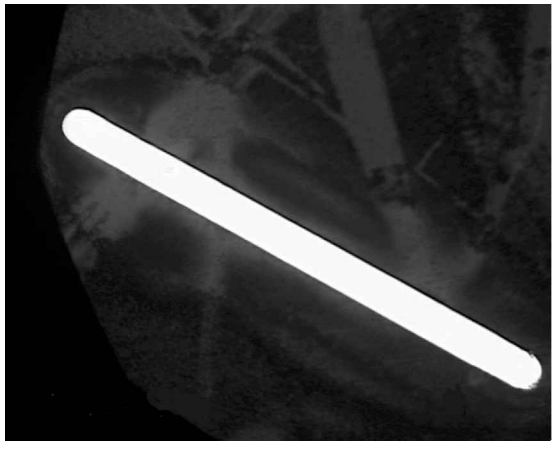

Bottom view

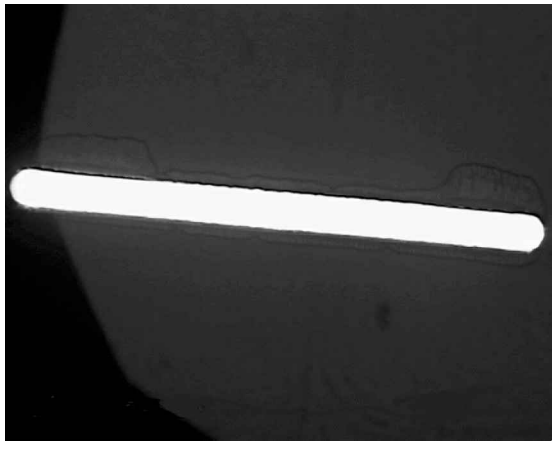

Top view

Fig. 5 Elliptical orifice 3G with hydraulic diameter 70 μm, machined using the double sided etching technique.

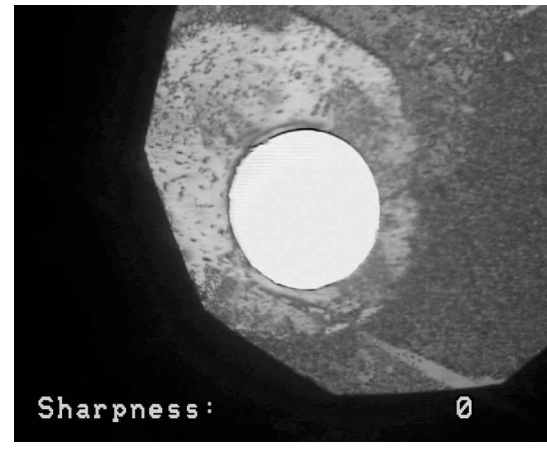

Bottom view

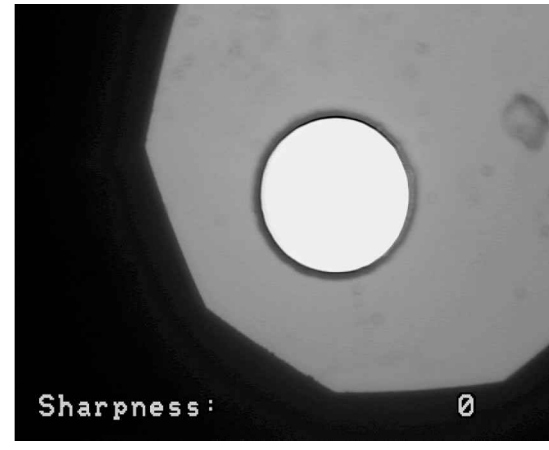

Top view

Fig. 6 Circular orifice 1G with diameter 70 μm, machined using the double-sided etching technique.

Results

Based on the experimental procedure for the measurement and correlation of hydrogen and helium leak detection just described, mass flow rates of these leaked species were measured by the TCD. These measurements resulted in raw data consisting of $\dot{m}_{\mathrm{He,actual}}$ and $\dot{m}_{\mathrm{H2,actual}}$ for various tank or upstream stagnation pressures p_t. These actual measurements of leak mass flow rates were used in Eq. (3) to determine the discharge coefficient associated with the various flow conditions. As is done in the typical HST, the stagnation temperature of the species gas upstream of the microorifice was assumed to correspond to the room temperature, $T_t = 291$ K. Discharge coefficients are typically determined for different orifice shapes as a function of orifice Reynolds number.[15] In the present case, it was possible for each flow condition, that is, each tank pressure p_t and each leaked species, to fix the Reynolds number for the orifice flow, given in terms of hydraulic diameter d_{hyd}:

$$Re(d_{\mathrm{hyd}}) = \frac{4\dot{m}_{(\mathrm{H2\ or\ He}),\ \mathrm{actual}}}{\pi d_{\mathrm{hyd}}\mu} \tag{5}$$

Note that under the present flow conditions it was determined that the Knudsen number was, at most, on the order of 0.006. Hence, for the flows through the microorifices examined in the present study, it was felt that the compressible flow remained in the continuum regime.

It was first sought to verify the choked flow condition in the microorifice because this condition is assumed in the standard HST and allows determination of the discharge coefficient defined in Eq. (3). One way to verify the choked flow condition was to show that, as the ratio of the orifice (or downstream) pressure p to the tank (or upstream) pressure p_t was decreased below the critical value given in Eq. (4), the mass flow rate approached a constant (choked) condition. This critical pressure ratio took the value 0.487

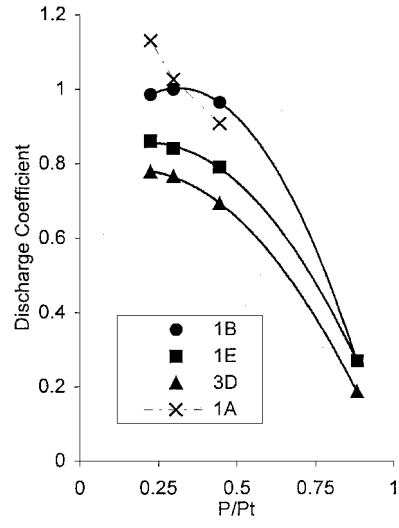

a)

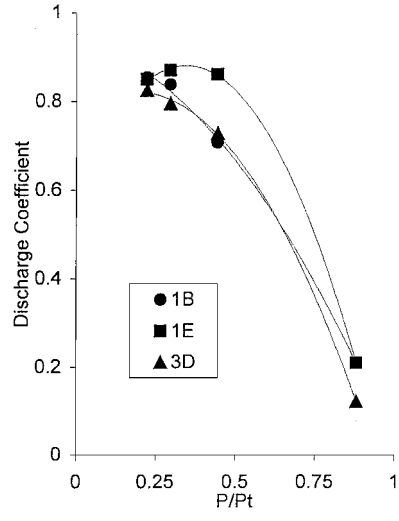

b)

Fig. 7 DC as a function of the pressure ratio p/p_t across the various microorifices for a) helium and b) hydrogen.

for helium and 0.528 for hydrogen. This type of verification was also performed by Jackson[8] for larger orifice flows.

Figures 7a and 7b contain graphs of discharge coefficient vs p/p_t to test the choked flow condition in the microorifices. Three orifices (four in the case of helium) were tested at four different upstream pressures: 3.45, 6.85, 10.25, and 13.65 atm. The behavior of several circular orifices and one elliptical orifice is shown, although similar results were observed for other orifices. In the case of hydrogen leakage, the larger orifices (1E and 3D) appeared to have flow rates and, hence, DCs, which asymptoted to a constant value as p/p_t was decreased below the critical value. For the very small circular orifice of diameter 15 μm (1B), however, the DC continuously increased with decreasing pressure ratio; this orifice was possibly not choked. In the case of helium, orifices 1E, 3D, and even 1B displayed choked flow behavior, that is, reaching limiting values of DC, although orifice 1B's discharge coefficient was suspiciously high. Furthermore, for helium, circular orifice 1A (with a 10-μm diameter) had a continuously increasing DC, even exceeding unity. We believe that this nonchoked flow behavior for the smaller orifices arose from the relatively small orifice thickness because the 1A and 1B orifices were about 70 μm in thickness compared to the 250-μm thicknesses of the other orifices. These findings were consistent with those of Jackson,[8] who observed that flows through knife-edged or thin orifices did not reach choked conditions under the theoretical pressure conditions for choked flow [Eq. (4)]. Although the reason for this nonchoked behavior may lie in diffusion of species through very thin wafer sections, it bears further study. The results

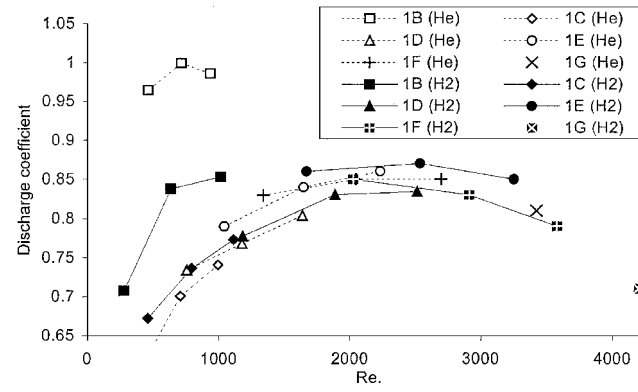

Fig. 8 DC as a function of Reynolds number for circular orifices, where helium flow measurements are open symbols and dashed lines and hydrogen measurements are filled symbols and solid lines.

shown for choked flow were replicated for all other (larger) orifices studied.

Figure 8 shows the variations in measured discharge coefficient with orifice Reynolds number, for both hydrogen and helium, and for circular orifices of various sizes. Data are included for all orifices for which choked flow was verified, in addition to orifice 1B. The unusually high DC values for helium flow through orifice 1B in Fig. 8 again suggest that choked flow may not have been completely attained here, consistent with the unusually high DC shown in Fig. 7a. In Fig. 8 the data suggested that, in general, the DCs for hydrogen were higher than for helium, although not significantly so. Whereas an increase in DC with increasing Reynolds number is typical of traditional nozzle- or channellike flows,[15] the slight dropoff in DC at Reynolds numbers above 2500 is less common for flow through larger circular tubes; it is reminiscent of the dropoff in DC observed in incompressible flows through sharper orifices, such as the square-edged orifices examined by Johansen.[16]

It is also important to quantify the effects of orifice shape on discharge coefficients in this study, particularly because most leaks arising in fuel or oxidizer tanks are more like slits or skewed ellipses rather than circular orifices. Figures 9a and 9b show comparisons of discharge coefficients for hydrogen and helium, respectively, for various orifices with comparable hydraulic diameters. For example, orifices 1D and 3D have about the same d_{hyd}. When hydraulic diameter and, hence, cross-sectional area were matched between a circular orifice and an elliptical or slit orifice, the slit systematically had a smaller DC than for the circular orifice and, hence, a lower mass flow rate for a given tank pressure. This result was consistent with elliptical slits containing a greater surface area than circles of the same cross-sectional area. Because the gas was exposed to a greater surface area as it flowed through an elliptical slit, viscous shear effects played a greater role, so that the effective dissipative effects were greater.

Figure 10 shows comparisons between the DCs for square orifice 2C and circular orifice 1C for hydrogen and helium, for a typical matched hydraulic diameter (20 μm). As with the comparison of the elliptical and circular orifices, the square orifices were found to have systematically lower discharge coefficients than for the circular orifice with the equivalent hydraulic diameter. These observations were similarly consistent with the surface area of a square hole being greater than that for a circular hole with matched hydraulic diameter, hence, implying the greater influence of viscous effects and a corresponding reduction in DC.

As noted in the Introduction, the process by which hydrogen leak rates are estimated using the standard HST method involves 1) testing the system at relatively low stagnation pressures with helium, 2) measuring the mass flow rate of leaked helium, 3) determining the effective orifice area A_{orifice} from the helium mass flow rate, assuming choked isentropic flow, and 4) estimating the hydrogen mass flow rate at higher pressures, assuming the same orifice area as for helium. This method was tested in the present set of experiments. Actual hydrogen leak rates for a given orifice were known, having been measured accurately via the TCD. These actual leak rates

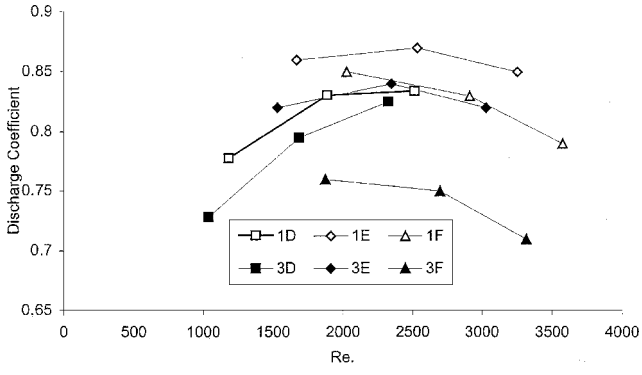

a)

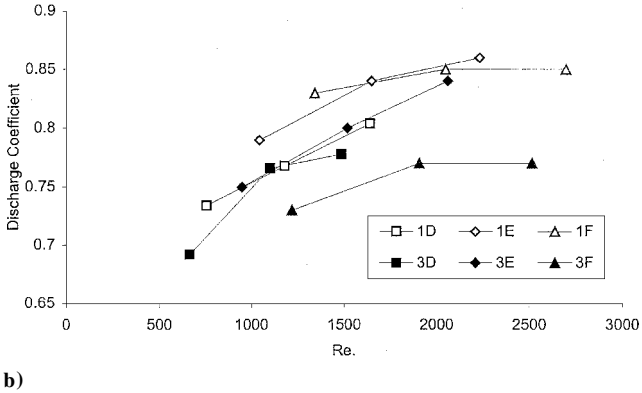

b)

Fig. 9 DC vs Reynolds number for circular orifices 1D, 1E, and 1F and slit orifices 3D, 3E, and 3F with the same cross-sectional areas, for both a) hydrogen and b) helium.

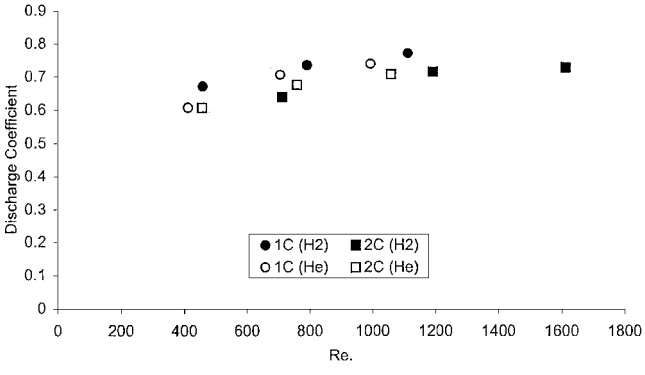

Fig. 10 DC vs Reynolds number for hydrogen and helium flows through circular orifice 1C and square orifice 2C with the same cross-sectional area.

at high tank pressures (13.65 atm) were compared with hydrogen leak rates that one would estimate, using the HST procedure, from measured helium leak rates at 6.85 atm. This comparison was made for a variety of orifices. The fact that the pressures of helium and hydrogen varied by a factor of two imposed a somewhat severe test of the HST, although these differences in pressures were not nearly as large as are often used in the HST, which can be of an order of magnitude. The helium leak rates for tank pressures of 3.45 atm were not used in the present HST comparison tests because the flow under these conditions did not always produce choked orifices.

Figure 11 plots the results of this HST validation, that is, the ratio of the actual to the HST-computed hydrogen mass flow rate as a function of the hydraulic diameter of the microorifice, for both circular and elliptical (slit) orifices. Results are also shown for very small orifices (10- and 15-μm diameter), where the choked flow assumption was questionable. Although in the case of these very small orifices the actual hydrogen leak rate was lower than that predicted by the HST method, in most fully choked orifice cases, the actual hydrogen leak rate exceeded the prediction. In the case

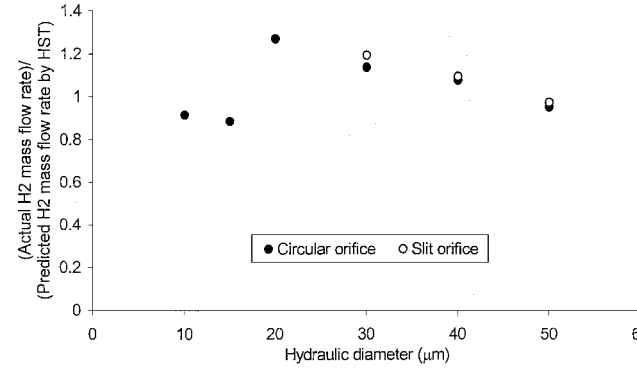

Fig. 11 Actual leak rates of H_2 from circular and slit orifices (for stagnation pressures of 13.65 atm) divided by H_2 leak rates predicted by the HST method (estimated from He leak rates for stagnation pressures of 6.85 atm) for various hydraulic diameters.

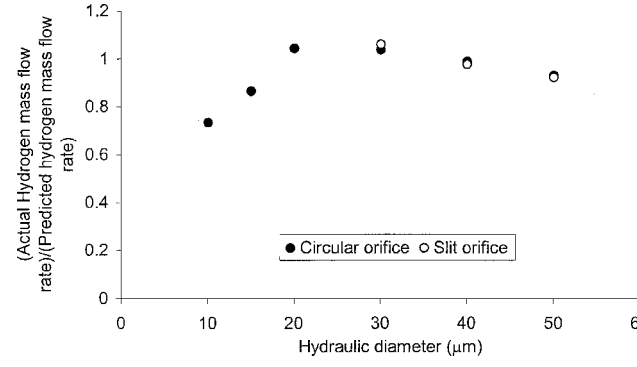

Fig. 12 Actual leak rates of H_2 from circular and slit orifices (for stagnation pressures of 13.65 atm) divided by H_2 leak rates predicted by the HST method (estimated from He leak rates for stagnation pressures of 13.65 atm) for various hydraulic diameters.

of a circular orifice with a 20-μm hydraulic diameter, the error in the HST method was about 27%, that is, the hydrogen leak rate was underpredicted by about 27%. The error in the HST method was actually slightly higher in the case of the slit than for the circular orifice, although this error diminished for larger leak orifice sizes. Because the actual HST procedure is usually performed where the stagnation pressure of helium test is much lower than the pressure for which the hydrogen leak rate is sought, by perhaps an order of magnitude or more, it is likely that the errors in the standard HST are much higher than the 27% underprediction observed here.

Figure 12 plots the results of a comparison between the actual hydrogen leak rate and that predicted by a modification to the HST method. In this comparison, predicted hydrogen leak rates were computed using the measured helium leak rates at 13.65 atm, the pressure of the desired hydrogen leak rate, rather than at 6.85 atm. This prediction was then compared with actual hydrogen leak rates at 13.65 atm. The predicted hydrogen leak rate was improved in comparison to the results in Fig. 11. The error between actual and predicted hydrogen leak rates was only a 6% underprediction in the worst case, for a circular orifice with a 30-μm diameter. This suggests that the accuracy of the HST for predicting hydrogen leak rates could be significantly improved if the helium leak tests were to be conducted at higher tank pressures, corresponding to more realistic hydrogen storage systems.

Conclusions

A systematic study of the relation between hydrogen and helium leak rates from micromachined orifices of prescribed sizes and shapes was conducted using a thermal conductivity detector. Micromachining challenges in terms of desired precision and sidewall shape profiles were mostly overcome in this study via optimized photolithography processes. Hence, it was possible to examine the differences in flow rates among accurately machined circular, square, and elliptical slit orifices. A variety of sets of data on orifice

DCs were taken, for orifice Reynolds numbers ranging from less than 500 to over 4000 and for stagnation to static pressure ratios ranging from about 4.5 (for a tank pressure of about 13.65 atm) down to about 1.1 (for a tank pressure of about 3.45 atm).

For most orifices under examination, except for extremely small ones (of hydraulic diameter of 15 μm or less), the flow in the orifices was verified to be choked. In the case of helium flow in particular, it was possible that the flow was not choked in the very small orifices. For the most part, DCs varied with Reynolds number, as has been documented in the past for much larger orifice or channellike flows, but with the notable exception that the DC tended to drop for Reynolds numbers above about 2500. DCs for square and elliptical slit orifices were systematically lower than for circular orifices; these trends correlate directly with the increased surface area within the orifice and, hence, with viscous effects.

Finally, comparisons were made between actual measured hydrogen leak rates and those which would be predicted from lower pressure helium leak rate measurements using the HST procedure. Although there may have been a slight discrepancy for the case of nonchoked, small orifices, by and large the HST method was seen to underpredict hydrogen leak rates, in some cases by nearly 30%. This error was found to be diminished, however, for larger leak orifice sizes. The error was also significantly reduced if the HST was conducted in helium at very high storage tank pressures, as high as for the desired hydrogen leak rates. This difference between helium and hydrogen flow rates is important to bear in mind in estimating actual hydrogen leakage in aerospace systems.

Acknowledgments

This work has been sponsored by NASA Dryden Flight Research Center under Grant NCC-2-374, with Neal Hass as Grant Monitor. The authors acknowledge the helpful advice of Chang-Jin Kim of the University of California, Los Angeles, Department of Mechanical and Aerospace Engineering and of Steve Franz of the University of California, Los Angeles, Nanotechnology Laboratory.

References

[1]Makel, D. B., Jansa, E. D., Bickmore, T. W., and Powers, W. T., "Automated Propellant Leak Detection," AIAA Paper 93-2590, June 1993.

[2]de Groot, W. A., "The Use of Spontaneous Raman Scattering for Hydrogen Leak Detection," AIAA Paper 94-2983, June 1994.

[3]Hunter, G. W., Makel, D. B., Jansa, E. D., Patterson, G., Cova, P. J., Liu, C. C., Wu, Q. H., and Powers, W. T., "A Hydrogen Leak Detection System for Aerospace and Commercial Applications," AIAA Paper 95-2645, July 1995.

[4]Barnes, H. L., and Makel, D. B., "Quantitative Leak Detection Using Microelectronic Hydrogen Sensors," AIAA Paper 95-2648, July 1995.

[5]Vincent, B., Jr., and Izquierdo, F., "Development of the Helium Signature Test for Orbiter Main Propulsion System Revalidation Between Flights," AIAA Paper 87-0293, Jan. 1987.

[6]Hass, N., Mizukami, M., Neal, B. A., St. John, C., Beil, R. J., and Griffin, T. P., "Propellant Feed System Leak Detection-Lessons Learned from the Linear Aerospike SR-71 Experiment (LASRE)," NASA TM-1999-206590, Nov. 1999.

[7]Mizukami, M., Corpening, G. P., Ray, R. J., Hass, N., Ennix, K. A., and Lazaroff, S. M., "Linear Aerospace SR-71 Experiment (LASRE): Aerospace Propulsion Hazard Mitigation Systems," AIAA Paper 98-3873, July 1998.

[8]Jackson, R. A., "The Compressible Discharge of Air Through Small Thick Plate Orifices," *Applied Scientific Research*, Sec. A, Vol. 13, 1964, pp. 241–248.

[9]Cunningham, R. G., "Orifice Meters with Supercritical Flow," *Transactions of the American Society of Mechanical Engineers*, Vol. 73, 1951, pp. 625–630.

[10]Anderson, J. D., *Hypersonic and High Temperature Gas Dynamics*, McGraw–Hill, New York, 1989, p. 22.

[11]Ho, C. M., and Tai, Y., "Micro-Electro-Mechanical-Systems (MEMS) and Fluid Flows," *Annual Review of Fluid Mechanics*, Vol. 30, 1998, pp. 579–612.

[12]Shih, J., Ho, C. M., Liu, J., and Tai, Y. C., "Monatomic and Polyatomic Gas Flow Through Uniform Microchannels," American Society of Mechanical Engineers, ASME MEMS, DSC-Vol. 59, Fairfield, NJ, 1996, pp. 197–203.

[13]Ayon, A. A., Lin, C. C., Braff, R. A., and Schmidt, M. A., "Etching Characteristics and Profile Control in a Time Multiplexed Inductively Coupled Plasma Etcher," Solid-State Sensor and Actuator Workshop, June 1998.

[14]Lee, I. D., "Hydrogen Leak Detection via Micromachined Orifices," M.S. Thesis, Dept. of Mechanical and Aerospace Engineering, Univ. of California, Los Angeles, 2001.

[15]Beckwith, T. G., Marangoni, R. D., and Lienhard, J. H., *Mechanical Measurements*, 5th ed., Addison Wesley Longman, Reading, MA, 1995, pp. 623–624.

[16]Johansen, F. C., "Flow Through Pipe Orifices at Low Reynolds Numbers," Aeronautical Research Committee, Research Publ. 1252, London, 1930.

M. Sichel
Associate Editor